In Situ Generation of Tunable Porosity Gradients in Hydrogel-Based Scaffolds for Microfluidic Cell Culture

*Aswan Al-Abboodi, Ricky Tjeung, Pauline M. Doran, Leslie Y. Yeo, James Friend, and Peggy Pui Yik Chan**

Compared with preformed anisotropic matrices, an anisotropic matrix that allows users to alter its properties and structure in situ after synthesis offers the important advantage of being able to mimic dynamic in vivo microenvironments, such as in tissues undergoing morphogenesis or in wounds undergoing tissue repair. In this study, porous gradients are generated in situ in a hydrogel comprising enzymatically crosslinked gelatin hydroxyphenylpropionic acid (GTN–HPA) conjugate and carboxylmethyl cellulose tyramine (CMC–TYR) conjugate. The GTN–HPA component acts as the backbone of the hydrogel, while CMC–TYR acts as a biocompatible sacrificial polymer. The hydrogel is then used to immobilize HT1080 human fibrosarcoma cells in a microfluidic chamber. After diffusion of a biocompatible cellulase enzyme through the hydrogel in a spatially controlled manner, selective digestion of the CMC component of the hydrogel by the cellulase gives rise to a porosity gradient in situ instead of requiring its formation during hydrogel synthesis as with other methods. The influence of this in situ tunable porosity gradient on the chemotactic response of cancer cells is subsequently studied both in the absence and presence of chemoattractant. This platform illustrates the potential of hydrogel-based microfluidics to mimic the 3D in vivo microenvironment for tissue engineering and diagnostic applications.

1. Introduction

Spatial anisotropy is common in the in vivo cellular microenvironment where cells and biomolecules are heterogeneously distributed within extracellular matrices (ECM), which possess spatial variations in structure and properties.[1] For example, bone is characterized by porosity gradients reflecting the presence of compact (porosity 5%–30%) and spongy (porosity 30%–90%) structures.[1] The ligament–cementum and cementum–dentin interfaces in teeth both consist of stiffness-graded interfaces.[2,3] Coronal cementum, a heterogeneous material comprising laminar cementum that is high in mineral content, and fibrous cementum that is high in organic content, thus possess a combination of chemical and physical gradients.[4] Examples of matrix gradients can also be found in liver, intestine, skin, and hemopoietic tissues.[5] Such spatially varying ECMs play important roles in the cellular microenvironment by defining boundaries between different tissue for morphogenesis, providing instructive signals to direct cell differentiation,[6,7] providing binding sites to growth factors and cytokines,[8] configuring cell shapes, directing cell movement, altering cell responses to growth factor signals, and regulating soluble signals through sequestration of growth factors.[5] Further, ECMs are highly dynamic and can be remodeled by the cells they are in contact with.[6] For instance, newly generated ECM after tissue injury regulates a series of cell processes to rebuild the tissue, which, in turn, serves to remodel the ECM to emulate normal tissue.[9]

Given the limitations in the ability of tissues to self-repair,[10–12] replacement tissues are often needed to treat defects arising as a result of traumatic injury or tumor resection. Most current tissue engineering approaches aim to recreate ECMs in the form of tissue scaffolds in order to replace malfunctioning or missing tissue.[13] It is well known that the bioactivity of a tissue scaffold is dependent on its ability to induce cell migration through the scaffold, and that such cell migration is required to facilitate tissue regeneration.[14] For example, it has been demonstrated that myofibroblast migration into collagen-GAG scaffolds is necessary for successful skin regeneration, while no regeneration was found in scaffold

A. Al-Abboodi
Department of Chemical Engineering
Monash University
Clayton, VIC 3800
A. Al-Abboodi
Australia Mico/Nanophysics Research Laboratory
RMIT University
Melbourne VIC 3000, Australia
R. Tjeung, Prof. L. Y. Yeo, Prof. J. Friend, Dr. P. P. Y.Chan
Mico/Nanophysics Research Laboratory
RMIT University
Melbourne, VIC 3000, Australia
E-mail: peggy.chan@rmit.edu.au
R. Tjeung, Prof. L. Y. Yeo, Prof. J. Friend, Dr. P. P. Y. Chan
Melbourne Centre for Nanofabrication
Australia National Fabrication Facility
Clayton, VIC 3168, Australia
Prof. P. M. Doran
Faculty of Science, Engineering & Technology
Swinburne University of Technology
Hawthorn, Melbourne VIC 3122, Australia

DOI: 10.1002/adhm.201400072

structures that retarded cellular migration.[14] Anisotropic biomaterials that mimic the heterogeneity of the in vivo microenvironment provide an opportunity to regulate cell migration, and are therefore attractive for tissue scaffold development and for studying various cell–matrix interactions including tissue regeneration, morphogenesis, and metastasis. Creating 3D rather than 2D anisotropic biomaterials is particularly attractive, as the dimensionality of the microenvironment is a critical factor for simulating in vivo conditions.[15]

Attempts have been made to synthesize preformed scaffolds possessing either a continuous change in porosity (i.e., a gradient structure) or a step-wise change in porosity (i.e., a graded structure).[16] For example, multiple tape casting of hydroxyapatite slurry containing polybutylmethacrylate porogens has been used followed by removal of the porogens via sintering;[17] however, such structures are prone to delamination defects at high sintering temperatures[17] and pore interconnectivity is low along the tape interfaces.[16] On the other hand, Muthutantri et al.[18] prepared graded porous structures by electrospraying zirconia and using the spraying time, sintering temperature, and sacrificial template to control the porosity; however, it is difficult to control the structural regularity of the resulting structure. Macchetta et al.[19] fabricated graded porous scaffolds by varying both the solid content of hydroxyapatite/tricalcium phosphate slurry and the freezing temperature, followed by sintering. Harley et al.[14] showed that preformed scaffolds with pore size gradients can be fabricated using a combination of spinning and rapid freezing techniques; however, it is generally difficult to control the temperature gradient in such freezing-based methods. All of these and other methods used to synthesize preformed scaffolds with pore size gradients or graded porosities are summarized in Miao and Sun.[16]

The versatility of microfluidic devices for spatially controlling cells and designing suitable patterns of cells and materials for drug discovery offers an attractive alternative to these conventional approaches.[20–22] In particular, microfluidics offers precise control over the configuration of stable concentration gradients to facilitate easy and accurate quantification of cell migration while requiring a much lower quantity of reagents and cells than larger-scale flow systems. The time required to dynamically mimic the in vivo variation of chemoattractant gradients is also drastically reduced due to the smaller characteristic length scales over which diffusive transport takes place in microfluidic channels.[22–24] In previous work, Kreppenhofer et al. demonstrated the fabrication of preformed scaffolds with porosity gradients in a microfluidic device using UV-crosslinkable butyl methacrylate (monomer), ethylene glycol dimethacrylate (crosslinker), 1-decanol (porogenic solvent), and cylohexanol solvent (porogen). In this method, two polymerization mixtures, one containing the porogen and the other containing the porogenic solvent, were pumped into a microfluidic chip from two inlets to create a gradient in the reaction chamber based on the density difference between the two mixtures, the density difference being controlled by the pumping flow rate. The gradient structure was then UV-polymerized followed by solvent drying to generate a porosity gradient with pore sizes of 0.1–0.5 μm[25]; however, this pore size range was too small for culture of mammalian cells with typical sizes of 15–25 μm.[26] He et al.[27] demonstrated that preformed poly(ethylene glycol)–diacrylate hydrogel with graded porosity can be generated in a microfluidic device using a combination of passive-pump-induced flow, evaporation-induced backflow, and freeze-drying. Typically, such methods for fabricating anisotropic matrices with preformed porosity gradients or graded porosity are laborious and require toxic organic solvents or freeze-drying, which are not suitable when cells are immobilized in situ at the time the pores are formed or modified. Moreover, to date, all of the anisotropic matrices produced with porosity gradients or graded porosity comprise preformed matrices that retain their original architecture and do not allow the pore structure to be generated or tuned in situ; they are unable, therefore, to reflect the dynamic nature of in vivo tissue. In contrast, an anisotropic matrix that allows porosity gradients to be generated or tuned in situ can provide more realistic biomimetic conditions to support cell–matrix interactions, leading to a better understanding of how cells interact with dynamic microenvironments such as those found in tissues undergoing early-phase synthesis or repair.

Seeding cells controllably and uniformly within a tissue scaffold[28–31] or microfluidic system,[32] while crucial for efficient culture, is nevertheless challenging. With preformed tissue scaffolds, it is often difficult to deliver cells deep into the center of the scaffold to achieve uniform cell seeding because of the hydrophobicity of the scaffold and its small pore size (typically 10–150 μm diameter) that imposes a large capillary resistance. The presence of a graded porous structure makes the situation more complex. Some investigators have attempted to achieve uniform cell seeding by seeding cells into cut sections of preformed porous gradient scaffolds.[33,34] For example, Dubruel et al.[35] seeded a graded porous structure by adding cells dropwise along the side that contained the larger pores and then flipping the structure after one day. The cells spread out to form a confluent monolayer on the side of the scaffold where the cells were seeded; however, cell migration throughout the thickness of the scaffold was not shown. Zhang et al.[36] fabricated preformed porous gradient scaffolds with large pore sizes of 150–500 μm using ice particles as porogens. Uniform cell seeding was achieved by seeding cells twice into the scaffold followed by shaking for 1 week. However, scaffolds with such large pores may not be suitable for many types of tissue; for instance, the optimum pore size for neovascularization is 5 μm, fibroblast ingrowth 5–15 μm, hepatocyte ingrowth 20 μm, skin regeneration 20–125 μm, and liver tissue regeneration 40–150 μm.[33] In addition, shaking the scaffold may subject the cells to undesirable levels of shear stress.

In the case of a preformed matrix with porosity gradient or graded porosity within a microchamber, cell seeding can be carried out by infusing a cell suspension into the matrix or by drawing a cell suspension from an external reservoir into the microchamber. As this is similar to how cells are seeded in 2D microfluidic culture systems,[32] the same cell seeding difficulties experienced in 2D microfluidics can be expected. In particular, the low cell seeding flow rates used to avoid a reduction in the cell viability often result in cells sedimenting in the reservoir and connection channels before reaching the microchamber.[32] Moreover, it is well known that the pore size of a matrix has a strong influence on cell seeding, in that cells preferentially adhere to smaller pores due to the availability of larger surface area.[37,38] For these reasons, it is therefore

extremely difficult to achieve uniform cell seeding in a preformed graded/gradient porous scaffold housed within a microchamber. The scarcity of cell migration studies in microfluidic devices with porous gradients[25,27] is likely due to these difficulties in achieving uniform cell seeding.

Here, we demonstrate a novel and facile method to generate continuous porosity and chemical gradients in situ in a hydrogel-based microfluidic device. As an example application of this system, we also demonstrate its use for studying cancer cell migration and chemotaxis in a dynamic microenvironment. To the best of our knowledge, such an in situ method for gradient development and control has not been previously reported. Further, this is the first study to show the collective effects of porosity and chemical gradients on cell migration. Our microfluidic device comprised a polydimethylsiloxane (PDMS) film covered glass slide with a series of cell culture chambers complete with inlet and outlet microchannels. This was used to generate a chemoattractant concentration gradient through a gelatin–hydroxyphenylpropionic acid (GTN–HPA)/carboxylmethyl cellulose-tyramine (GC) hydrogel with tunable porosity in situ, thus mimicking a 3D in vivo culture environment. The hydrogel was prepared using two polymer conjugates, namely GTN–HPA conjugate and carboxylmethyl cellulose–tyramine (CMC–TYR) conjugate. The GTN–HPA conjugate served as the backbone of the hydrogel and contained Arg-Gly-Asp (RGD) peptides that provide adhesive ligands for cell adhesion.[39] The CMC–TYR conjugate, which contains CMC, a low-cost cellulose derivative approved by the US Food and Drug Administration (FDA) for pharmaceutical use,[40] was used as the sacrificial polymer in the GC hydrogel.[41] The GTN–HPA and CMC–TYR conjugates were crosslinked via oxidative coupling of the phenol moieties catalyzed by horseradish peroxidase (HRP) enzyme to yield an in situ porous hydrogel; the enzyme-mediated crosslinking process can be performed in mild conditions, that is, at room temperature and in an aqueous environment. The cells were premixed with the GC hydrogel precursor solution and simply injected into the microfluidic cell culture chamber; the cells were thereby immobilized at uniform cell density within the scaffold as the hydrogel was crosslinked inside the microchamber.[41] We note that the hydrogel may be injected to fill a microchamber of arbitrary shape. The resulting GC hydrogel is compatible with a range of microanalysis and nanocharacterization techniques, including laser scanning confocal microscopy (LSCM), environmental scanning electron microscopy, focused ion beam milling, and electron scanning microscopy (FIB/SEM).[42]

To alter the pore size of the crosslinked GC hydrogel, a biocompatible enzyme, cellulase, was added to the hydrogel to digest the sacrificial CMC component of the hydrogel. The cellulase used was extracted from *Trichoderma longibrachiatum*, which is approved by the US FDA and common in the food industry.[41] We have previously demonstrated that cellulase digests CMC selectively while remaining inert to mammalian cells and native ECM both in vitro and in vivo.[41] The GC hydrogel-based microfluidic device developed in this work was used to study human fibrosarcoma cells (HT1080) as these cells can be readily propagated and are suitable as an invasive cancer cell model.[43] The results demonstrate that physicochemical-gradient-induced cell movement and HT1080 cell behavior can be successfully controlled in situ with minimal cost or special expertise. The device thus allows users to tailor the scaffold in situ to study cellular responses in a dynamic biomimetic microenvironment. In contrast to static culture systems where the structural parameters cannot be changed during the reaction (cell migration), such a dynamic culture system is, in principle, akin to a dynamic reactor that allows the user to controllably vary the structural parameters, namely, the porosity, in particular, during the reaction. Moreover, maintaining cell growth inside the porous hydrogel structure provides a route to its potential use in tissue scaffolding.

2. Experimental Section

2.1. Materials

Gelatin ($\bar{M}_w$ = 80–140 kDa) and HRP (100 units mg^{-1}) were obtained from Wako Pure Chemical Industries (Osaka, Japan). 3,4-hydroxyphenylpropionic acid (HPA), *N*-hydroxysuccinimide (NHS), 1-ethyl-3-(3-dimethylaminopropyl)-carbodiimide hydrochloride (EDC), CMC ($\bar{M}_w$ = 90 kDa), cellulase from *Trichoderma longibrachiatum*, fluoresceinamine isomer I, tyramine hydrochloride (TYR), albumin fluoresein isothiocyanate conjugate (FITC-BSA), and deuterium oxide (D_2O) were purchased from Sigma–Aldrich (Sydney, NSW, Australia). Hydrogen peroxide (H_2O_2) was acquired from Merck (Kilsyth, VIC, Australia), a LIVE/DEAD Viability Kit for determining mammalian cell viability was obtained from Life Technologies (Mulgrave, VIC, Australia), and PDMS (Sylgard 184) was purchased from Dow Corning (Midland, MI, USA).

2.2. Microfluidic Device Fabrication and Assembly

The microfluidic device was constructed from a PDMS layer bonded onto a microscope slide. PDMS was preferred for device fabrication since it is biocompatible and possesses good optical transparency.[40] **Figure 1** illustrates the step-by-step procedure for the microfluidic device fabrication and assembly. The desired pattern was designed using AutoCAD software (Autodesk Inc., San Rafael, CA), from which the master mold was printed using a 3D printer (Objet Eden 3D, Stratasys Inc., Eden Prairie, MN) and UV-curable polymeric material (Objet FullCure720). 3D printing was chosen due to its ability to overcome the main limitation of conventional photolithographic techniques; that is, the facile construction of microstructures with various thicknesses in a single run. This technique shortens the fabrication time and eliminates the complexity associated with multiple runs or masks. The mold consisted of one main chamber, two inlet reservoirs, and several microchannels: the dimensions of these are listed in **Table 1**. A schematic diagram of the master mold is shown in **Figure 2**. The PDMS layer was then fabricated using standard soft lithography,[44] which can be carried out without the need for routine access to a clean room.[21] The PDMS layer was subsequently removed from the master mold after thermal curing at 80 °C for 30 min and plasma treatment (Harrick Plasma, Ithaca, NY) for 3 min before being irreversibly sealed to the microscope slide.

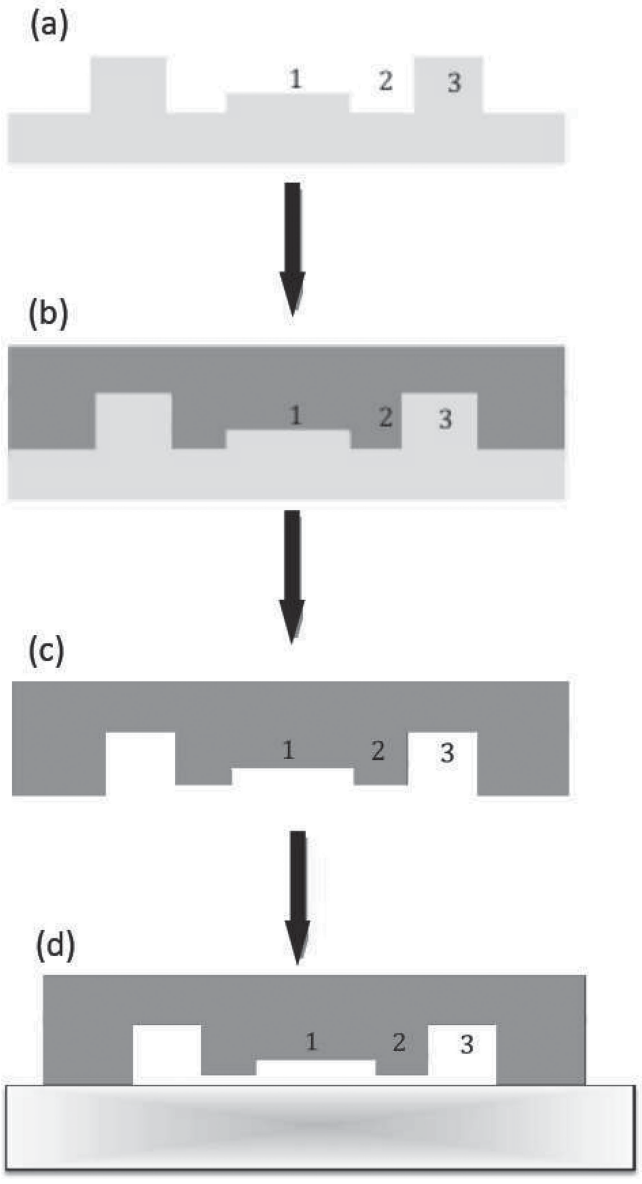

Figure 1. Fabrication of the PDMS microfluidic device. The schematic diagrams (not to scale) are shown in cross-sectional view. a) A transparent polymeric (Objet FullCure720, Stratasys Inc., Eden Prairie, MN) master mold (light gray structure) was designed using AutoCAD software and constructed using a 3D printer. The mold has structures with three different heights that were constructed at the same time: 1) 300 µm, 2) 200 µm, and 3) 500 µm. b) Microchannels in PDMS were constructed using soft lithography[44] by casting the PDMS (dark gray structure) utilizing the master mold. c) After curing, the PDMS layer with the imprinted microchannel structures was peeled off from the mold. d) The PDMS layer was then surface treated using an oxygen plasma system and subsequently bonded onto a glass slide (bottom structure) to construct the microfluidic device.

2.3. Synthesis of the Hydrogel Precursor

GTN–HPA conjugates were prepared using the procedure described by Kurisawa and co-workers.[39,45,46] using a carbodiimide ester-mediated coupling reaction. Fluorescently labeled Gtn–HPA conjugates were prepared by activating the –COOH group of GTN–HPA (10 g) by NHS and EDC at pH 4.8 for 15 min in 500 mL of MilliQ water. To this solution, fluoresceinamine isomer I (0.23×10^{-6} M) in methanol (2 mL) was added dropwise while stirring overnight in the dark. The products were dialyzed against MilliQ water for 3 d followed by lyophilization. The CMC–TYR conjugates were prepared as described previously.[42] In brief, CMC (5 g) and TYR (0.864 g) were added to 250 mL of MilliQ water. NHS (0.573 g) and EDC (0.955 g) were then added to the solution and stirred overnight at room temperature and pH 4.7. The products were subsequently purified by dialysis against 100×10^{-3} M NaCl for 2 d, followed by 25% ethanol and water in sequence for 2 d each. Finally, the purified products were lyophilized. The synthesis of GTN–HPA and CMC–TYR are illustrated in **Figure 3**a,b, respectively. The conjugation of TYR onto CMC was confirmed by ^{1}H NMR (D_2O). Two peaks were detected at 7.1 and 6.8 ppm, corresponding to the phenyl protons associated with the aromatic ring structure present on tyramine, thus confirming the successful conjugation of TYR onto CMC.

Table 1. List of microstructures and their dimensions in the microfluidic device.

Component	Functions	Planar dimensions (width × length × height) [mm]
1	Two inlet reservoirs	8 × 8 × 0.5
2	One main chamber	15 × 15 × 0.3
3	Two microchannels connecting the inlet reservoirs to the main chamber	0.2 × 3.5 × 0.2
4	One microchannel for each of the inlet reservoirs for flushing purposes	0.3 × 8 × 0.2
5	One microchannel for the main reservoir for flushing purposes	0.3 × 5 × 0.2

2.4. Formation of the Porous Hydrogel

GTN–HPA and CMC–TYR solutions were prepared by dissolving 5% (w/v) GTN–HPA and 5% (w/v) CMC–TYR in phosphate buffer solution (PBS). The solutions were immediately sterilized using syringe filters. To prepare the GC hydrogel, the hydrogel precursor solution was prepared by mixing GTN–HPA solution and CMC–TYR conjugate solution with a weight ratio of 80:20, respectively. An enzymatic oxidative coupling reaction was induced by adding horseradish peroxidase (HRP, catalyst) and diluted H_2O_2 (oxidant) at final concentrations of 3.86 unit L^{-1} and 49.8×10^{-6} M, respectively. The solution was then vortexed vigorously for a few seconds. Forty microliters of the solution was subsequently injected directly into the main chamber of the microfluidic device and allowed to gelate. In general, specific volumes of scaffold material, with or without cells, could be introduced into the chamber without the need for alternative perfusion loading steps. After gelation, a hydrogel with homogeneous porous structure was formed inside the main chamber (Figure 3c). Gelation of the hydrogel was studied using an oscillatory rheometry technique as described previously.[39] The gel point, also known as the gelation time, is defined as the point

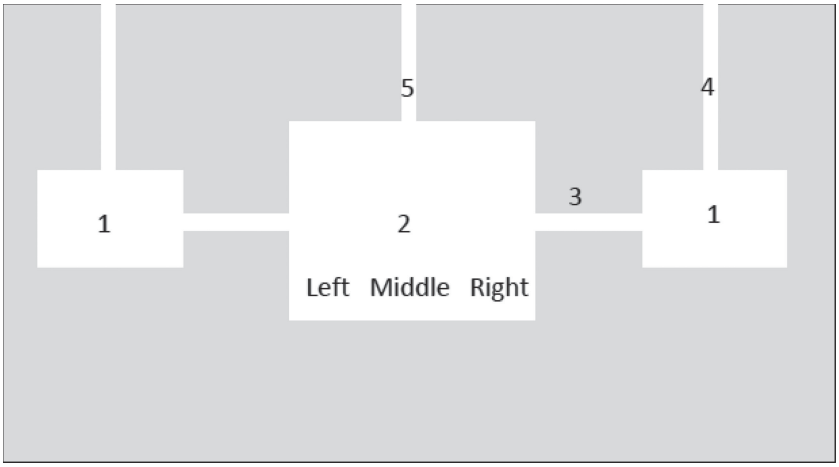

Figure 2. Top view schematic of the PDMS microfluidic device (not to scale). The device comprises 1) two inlet reservoirs (8 × 8 mm) for solution injection, 2) one main chamber (15 mm × 15 mm) for cell culture, 3) two microchannels (3.5 mm × 0.2 mm) connecting the main chamber with the two inlet reservoirs, 4) two microchannel (0.3 mm × 8 mm) inlets, one to each inlet reservoir, for flushing purposes, and 5) one microchannel (0.3 mm × 5 mm) inlet to the main chamber. The left, middle, and right regions were located 3, 9, and 12 mm, respectively, from the left side of the 15-mm long main chamber.

where the storage modulus and loss modulus crossover and was found to be ≈597 s.

2.5. Generation and Characterization of the Concentration Gradient

The feasibility of generating a protein concentration gradient was evaluated. It is well known that the mobility of protein in a gel is largely dependent on the molecular weight and isoelectric point of the protein.[47] FITC–BSA ($\bar{M}_w$ = 66 389) was selected as a model fluorescent protein because BSA has been widely used in various diffusion studies and is well characterized;[23,48–50] the molecular weight of FITC–BSA is similar to that of the high- molecular-weight fraction of cellulase ($\bar{M}_w$ = 63 000);[51] the isoelectric point of FITC–BSA (pH 4.7)[52] is also similar to that of cellulase (pH 3.9–4.52).[53] As such, we expect the mobility of the two proteins to be similar. To generate a concentration gradient

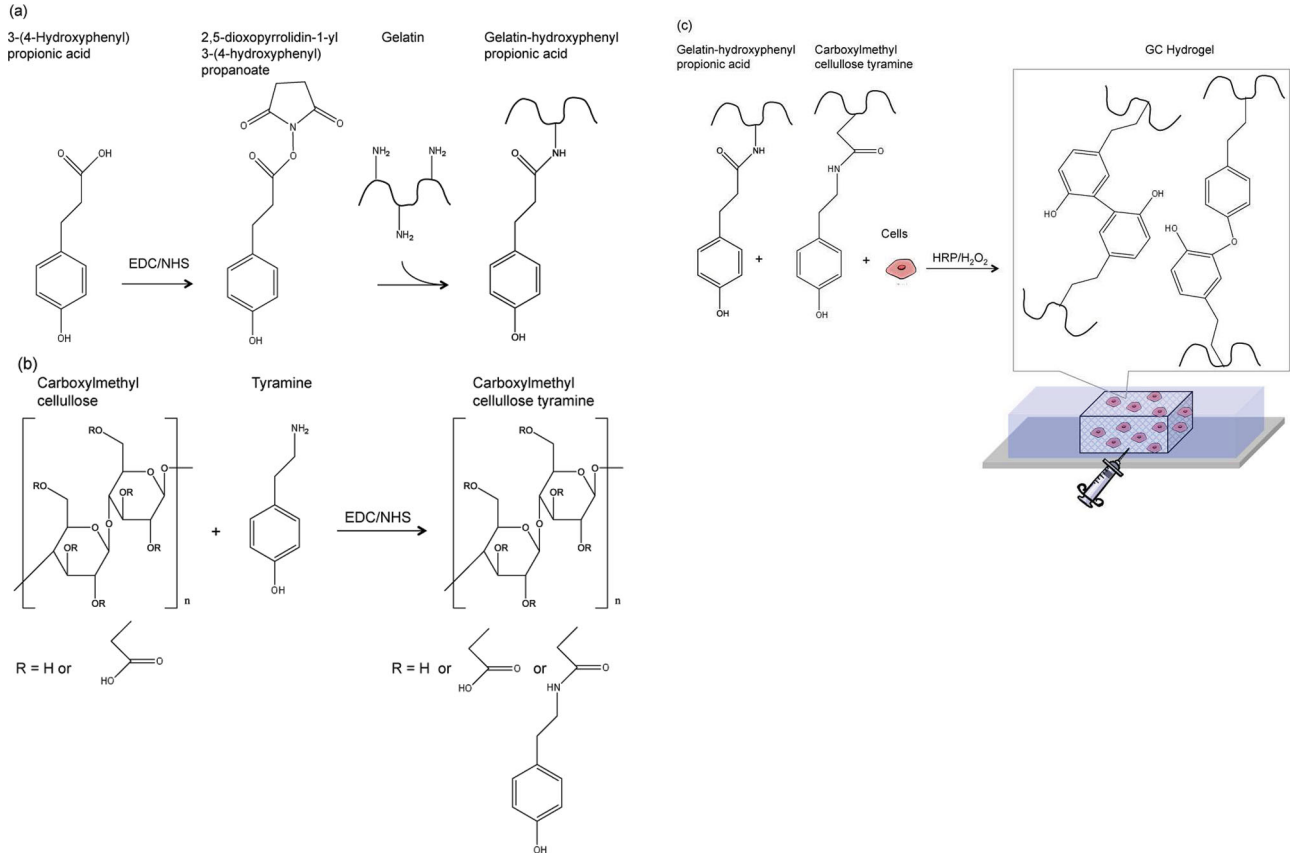

Figure 3. Synthesis scheme of a) the GTN–HPA conjugates, and b) the CMC–TYR conjugates. c) Preparation of the GC hydrogel in the microchamber. A mixture of GTN–HPA, CMC–TYR, HRP catalyst, and diluted H_2O_2 oxidant was injected into the microchamber and allowed to form a porous hydrogel. When cells were added to the mixture, the cells were immobilized in the gel simultaneously.

along the hydrogel, the left inlet reservoir was injected with 10 μL of FITC–BSA at a concentration of 10×10^{-6} M in PBS solution. The right reservoir was injected with 10 μL of PBS. A FITC–BSA concentration gradient was then allowed to form by diffusion over a period of 72 h. Spent solutions were replaced with fresh solutions daily. To quantitatively analyze the concentration gradient of biomolecules that diffused from the right or left reservoirs to the main chamber, the mean fluorescence intensity of FITC–BSA was measured in seven different regions: 0, 2.5, 5, 7.5, 10, 12.5, 15 mm from the left side of the 15-mm long main chamber. The fluorescence light intensity (FI) emitted by the FITC–BSA solution in each region was traced using LCSM (Nikon A1Rsi, Tokyo, Japan) to determine visually if the FITC–BSA diffused through the hydrogel. The distribution of FITC–BSA in the confocal images was quantified using ImageJ (v1.44o; National Institutes of Health, Bethesda, MD). In particular, the normalized fluorescence intensity (NFI) was calculated from

$$\mathrm{NFI} = \frac{\mathrm{FI}_{\mathrm{sample}} - \mathrm{FI}_{\mathrm{background}}}{\mathrm{FI}_{\mathrm{saturation}} - \mathrm{FI}_{\mathrm{background}}} \times 100\% \quad (1)$$

where $\mathrm{FI}_{\mathrm{sample}}$ is the fluorescence intensity obtained from the sample containing the FITC–BSA gradient, $\mathrm{FI}_{\mathrm{background}}$ is the fluorescence intensity obtained by measuring the microfluidic device filled with PBS alone, and $\mathrm{FI}_{\mathrm{saturation}}$ is the saturation fluorescence intensity obtained by measuring the brightest sample which is that in the left reservoir containing FITC–BSA only.

2.6. Generation of GC Hydrogel with Continuous Porosity Gradient

To generate a continuous porosity gradient along the hydrogel, the left inlet reservoir was injected with 10 μL of cellulase enzyme solution at a concentration of 0.1 units mL^{-1}, while the right inlet reservoir was injected with 10 μL of PBS. Both solutions were added 2 h after gelation of the hydrogel. Spent solutions in the reservoirs were replaced with fresh solutions daily. The microfluidic device was then incubated at 37 °C for 3 d to allow the cellulase enzyme to diffuse into the hydrogel to form a concentration gradient, thus allowing the enzyme to digest the CMC–TYR and create a porosity gradient within the matrix as illustrated in **Figure 4**. LSCM images were acquired 2 and 72 h after hydrogel gelation to visualize the hydrogel structure inside the main chamber.

2.7. Characterization of the Hydrogel Pore Gradient

To quantitatively analyze the porous gradient in the hydrogel from the right or left of the main chamber, the median pore diameter and porosity were measured in three different regions along the hydrated hydrogel in the main chamber. These three regions, left, middle and right, were located 3, 9, and 12 mm, respectively, from the left side of the 15-mm long main chamber. LSCM images were obtained at random locations within each of the three different regions. Analysis of pore size and porosity was then carried out at five different regions along the hydrogel

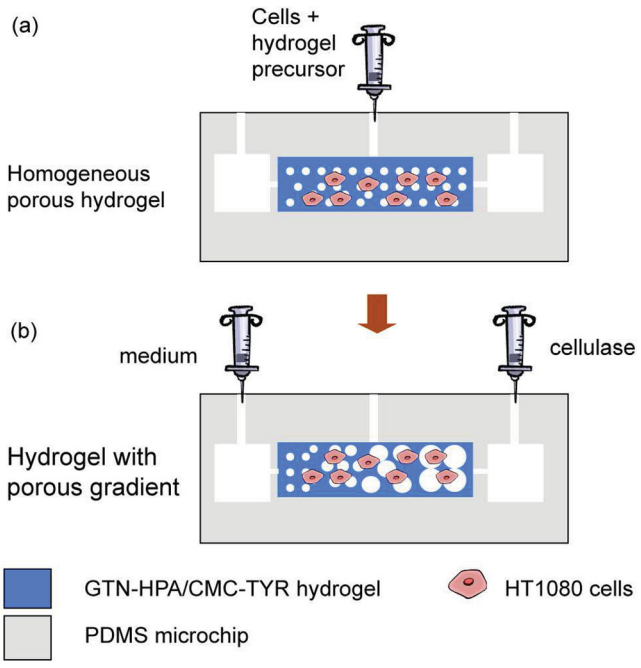

Figure 4. Schematic diagram (not to scale) illustrating the process of porosity gradient generation in the microfluidic device, which consisted of a PDMS layer imprinted with the microchannel structures bonded to a glass slide. a) The main chamber was injected with a mixture of GTN–HPA/CMC–TYR hydrogel precursor. The hydrogel was subsequently allowed to gelate within the chamber to form a homogeneous porous structure. Cells could be added to the mixture and injected to the main chamber as a single injection, thereby immobilized in the gel simultaneously as the hydrogel was gelated. b) To generate a porosity gradient, cellulase was injected into one of the inlet reservoirs while medium was injected into the other in order to generate a cellulase concentration gradient along the hydrogel in the main chamber. Digestion of the CMC–TYR component of the hydrogel by the cellulase then gave rise to larger pores in the cellulase-rich regions. Cell migration was monitored periodically.

using the previously described methods,[42] the five regions being located at 2.5, 5, 7.5, 10, and 12.5 mm from the left side of the main chamber. All LSCM analyses were performed using ImageJ.

2.8. Cell Culture

Invasive human fibrosarcoma HT1800 cells (Sigma–Aldrich) were cultivated in high-glucose Dulbecco's modified Eagle medium (DMEM; Sigma–Aldrich) supplemented with 10% (v/v) inactivated fetal bovine serum (FBS; Gibco, Life Technologies, Mulgrave, VIC, Australia) and 100 μg mL^{-1} penicillin–streptomycin at 37 °C in a 5% CO_2 humidified incubator. The cells were seeded onto a tissue culture flask for 3 d before harvesting. The medium was removed when the cells reached 80% confluency. The cells were subsequently washed with PBS buffer and detached using 0.25% trypsin (Gibco).

2.9. Cell Migration Study

Immediately after their fabrication, the microfluidic devices were sterilized by injecting the chambers and microchannels

with 70% ethanol followed by rinsing with sterile PBS under antiseptic conditions. The GTN–HPA and CMC–TYR solutions were prepared by dissolving 5% (w/v) GTN–HPA and 5% (w/v) CMC–TYR in serum-free DMEM, respectively, and immediately sterilized using syringe filters. To synthesize the GC hydrogel, the hydrogel precursor solution was prepared by mixing GTN–HPA solution and CMC–TYR conjugate solution using a weight ratio of 80:20, respectively. Three cases, which we describe below, were investigated in the cell migration study. In each configuration, a mixture containing 40 μL of GTN–HPA/CMC–TYR hydrogel precursor solution, HRP catalyst, dilute H_2O_2 oxidant, and 1×10^3 HT1080 cells were injected into the main chamber of the microfluidic device and allowed to gelate within 10 min.

2.9.1. Case 1: Cell Migration Along a Chemoattractant Gradient in the Absence of a Porosity Gradient

Here, chemotaxis of HT1080 cells was studied using the microfluidic device with a chemoattractant concentration gradient within the homogeneous porous structure. Twelve hours after hydrogel gelation, the left inlet reservoir was injected with 10 μL of serum-free DMEM, while the right inlet reservoir was injected with 10 μL of FBS. The FBS concentration gradient was subsequently allowed to form by diffusion. Spent solutions in the reservoirs were replaced with fresh solutions daily. The microfluidic device was incubated at 37 °C in a humidified incubator. Cell migration was monitored at 12, 24, 48, and 72 h after hydrogel gelation. LSCM microscopy images were acquired from the three regions of the main chamber (left, middle, and right) described above. The hydrogels were lyophilized and subsequently visualized using optical microscopy.

2.9.2. Case 2: Cell Migration Along a Porosity Gradient with No Chemoattractant Gradient

In this case, HT1080 migration was studied using the microfluidic device with changing porosity. Immediately after hydrogel gelation, the left and right inlet reservoirs were each injected with 10 μL of DMEM containing 10% FBS and incubated at 37 °C such that a homogeneous chemoattractant concentration was established in the main chamber, that is, no gradient of chemoattractant was present. After 12 h of equilibration, the solution in the left inlet reservoir was replaced with 10 μL of DMEM containing cellulase (0.1 units mL^{-1}) and 10% FBS, while the solution in the right inlet reservoir was replaced with 10 μL of fresh DMEM containing only 10% FBS. A cellulase concentration gradient was allowed to form via diffusion in order to generate a porosity gradient along the hydrogel. Spent solutions in the reservoirs were replaced with fresh solutions daily. The microfluidic device was incubated at 37 °C. Cell migration was monitored as described for Case 1.

2.9.3. Case 3: Cell Migration Along a Porosity Gradient in the Presence of a Chemoattractant Gradient

Here, HT1080 cell migration was studied using the microfluidic device under the influence of both changing porosity and a chemoattractant gradient. Immediately after hydrogel gelation, the left inlet reservoir was injected with 10 μL of serum-free DMEM containing cellulase (0.1 units mL^{-1}), while the right inlet reservoir was injected with 10 μL of FBS. A cellulase concentration gradient was allowed to form by diffusion in order to generate a porosity gradient along the hydrogel. At the same time, an FBS concentration gradient was also allowed to form in the opposite direction by diffusion. Spent solutions in the reservoirs were replaced with fresh solutions daily. The microfluidic device was incubated at 37 °C. Cell migration was monitored as described for Case 1.

2.10. Cell Viability Assay

Cell viability within the cell culture chamber was assessed using the LIVE/DEAD Viability Kit. Stained cells inside the culture chamber were imaged using LSCM to monitor cell migration. The number of viable encapsulated HT1080 cells was quantified by cell counting in the three regions of the main cell chamber (left, middle, and right) described above. The results were averaged and normalized with respect to the image area.

2.11. Statistics

Quantitative results are presented as mean ± standard deviation. Multiple groups of data were compared using one-way analysis of variance (ANOVA) and two groups of data were compared using the Student's *t*-test. All experiments were performed at least four times.

3. Results and Discussion

3.1. Concentration Gradient Analysis

Figure 5a illustrates the set-up used to generate a concentration gradient within the porous GC hydrogel in situ across the main chamber of the microfluidic device. The concentration gradient generated in the hydrogel can be observed from the distribution of fluorescently labeled protein (FITC–BSA) shown in Figure 5b and plotted in Figure 5c. The fluorescence intensity was strongest in the regions of the main chamber close to the left reservoir and gradually decreased toward the middle and right regions. This is also reflected in the normalized fluorescence intensity measured across the regions, where the normalized fluorescence intensity decreased toward the middle and right regions after 24 h ($p < 0.0001$, $n = 6$), 48 h ($p < 0.0001$, $n = 6$) and 72 h ($p < 0.0001$, $n = 6$) as seen in Figure 5c.

3.2. Characterization of the Continuous Porosity Gradient

Figure 4 illustrates the steps involved in generating an in situ continuous porosity gradient in the microfluidic device. Hydrogel precursor solution was first injected into the main chamber and allowed to crosslink to form homogeneous porous hydrogel within 10 min. Diluted cellulase was added to the left

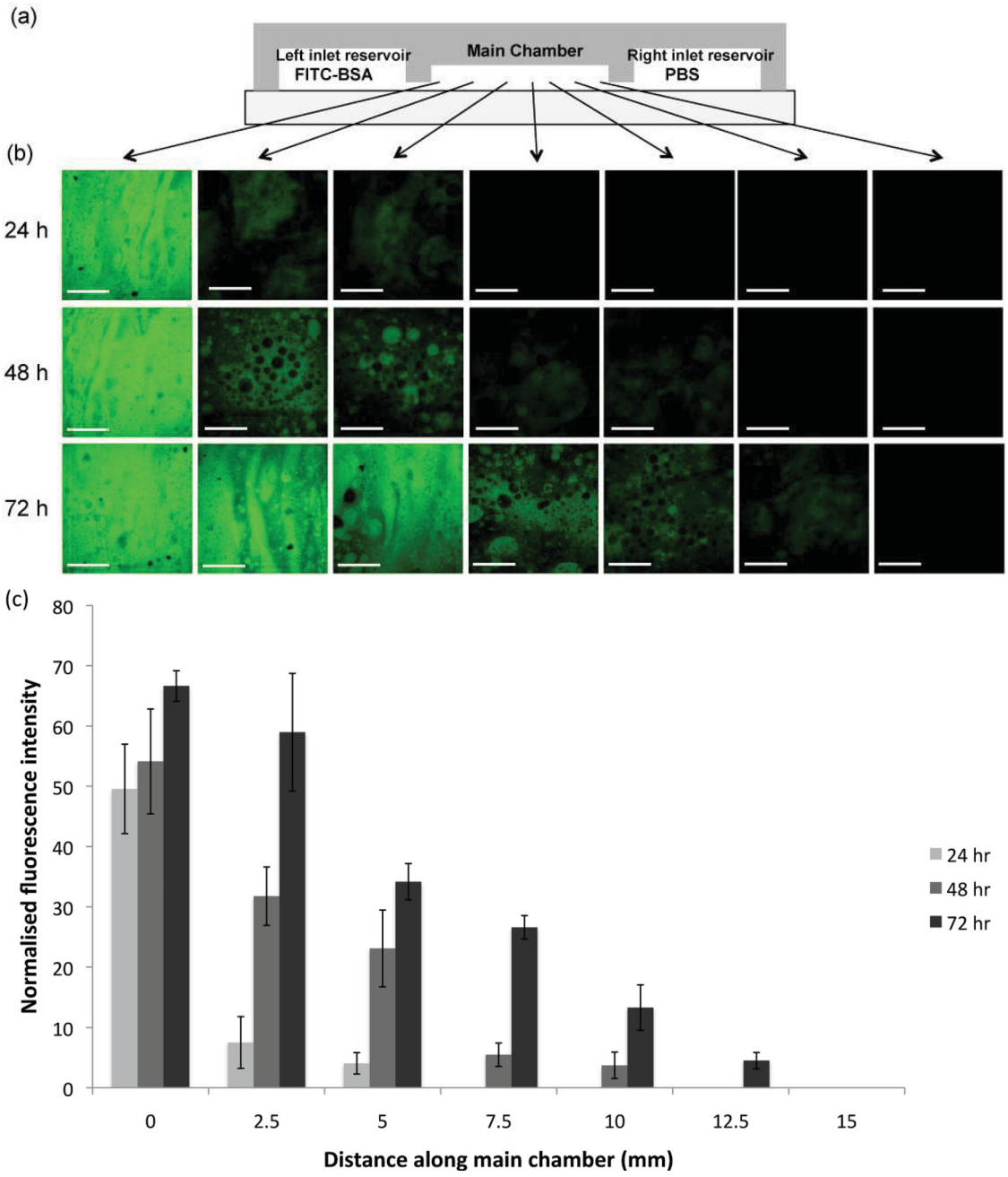

Figure 5. a) Schematic of the device used for the preliminary diffusion tests (not to scale). b) An FITC–BSA concentration gradient was generated across seven different regions in the main chamber. Scale bars represent 50 µm. c) Normalized fluorescence intensity of FITC–BSA in the seven regions from left to right of the porous hydrogel in the main chamber. The error bars represent the standard deviation.

inlet reservoir, while pure PBS solution was added to the right reservoir to generate a cellulase concentration gradient across the hydrogel by diffusion. The porous gradient then formed as the CMC component of the GC hydrogel was digested by the cellulase enzyme that diffused through the hydrogel, thereby opening larger pores in regions that were richer in cellulase. This enzymatic pore digestion process can be performed under physiological conditions (i.e., aqueous environment, room temperature, physiological pH) and in the presence of cells, and circumvents the need for toxic pore-etching reagents and freeze-drying typical in the conventional processes briefly described in Section 1. Therefore, the current process can be performed after microfluidic device construction and after cell immobilization.

For visualization, fluorescently labeled polymer conjugates were used for hydrogel formation, and the cellulase treatment was made to the hydrogel 2 h after gelation. The process of porosity gradient formation was monitored over a 72-h period using LSCM. The representative LSCM images in **Figure 6** show the morphology of the hydrated hydrogel

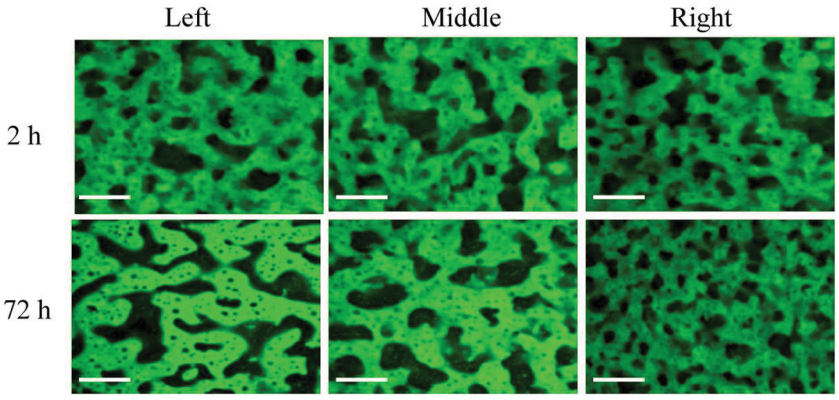

Figure 6. Variation in the pore size in three different regions (left, middle, and right) along the main chamber, cellulase enzyme was injected in the left reservoir at 2 h after gelation. Top row LSCM images show the porous structure after 2 h of gelation and before cellulase treatment. Bottom row LSCM images show the cellulase-treated porous structure after 72 h. The left, middle, and right regions were located 3, 9, and 12 mm, respectively, from the left side of the 15-mm long main chamber as depicted in Figure 2. Scale bars represent a length of 50 µm.

porous structures in the main chamber. The images obtained 2 h after gelation, these images reveal that the hydrogel possessed a homogeneous interconnected porous structure prior to cellulase digestion. Such interconnected porous structures facilitate oxygen and fluid exchange as well as cell migration throughout the hydrogel,[54] and are therefore advantageous for effective microfluidic cell culture. At 72 h after gelation, a gradual decrease in pore size across the chamber from left to right could be observed after cellulase digestion, thus demonstrating the feasibility of this approach for in situ porosity gradient generation in crosslinked hydrogel.

Figure 7 shows that, at day 0, the pore size (p = 0.66, n = 6) and porosity (p = 0.99, n = 6) were homogeneous across the hydrogel prior to cellulase treatment. After cellulase treatment at day 3, the pore sizes and porosity at regions located 2.5 and 5 mm from the left side of the main chamber were, on average statistically larger than those in the same regions at day 0, reflecting digestion of the sacrificial polymer by cellulase, which opened up larger pore structures. In addition, the pore size (p = 0.0001, n = 6) and porosity (p = 0.0013, n = 6) were larger in the regions of the main chamber close to the left reservoir (2.5 and 5 mm) and gradually decreased toward the middle (7.5 mm) and right regions (10 and 12.5 mm), thus demonstrating that an in situ porosity gradient was generated across the main chamber by the cellulase treatment.

3.3. Cell Migration

3.3.1. Case 1: Cell Migration Along a Chemoattractant Gradient in the Absence of a Porosity Gradient

Chemotaxis—the phenomenon of cell migration towards a soluble attractant under the influence of a concentration gradient[55]—is an important process in cancer metastasis, inflammatory disease, and tissue maintenance and restoration.[8,56] Although several culture systems are commercially available for chemotaxis studies, these systems often suffer from poor reliability and limited processing capacity. For example, the Dunn chemotaxis chamber permits only one condition to be studied at one time,[57] whereas the Boyden chamber requires laborious sample processing steps and does not permit real-time cell monitoring.[57,58]

Here, we demonstrate the use of the GC hydrogel-based microfluidic device for a chemotaxis assay. In particular, the migration of cells through a porous matrix in response to a varying chemoattractant concentration was investigated in real time. In Case 1, the hydrogel was not degraded by the cellulase enzyme and hence a uniform porosity was maintained throughout the scaffold. This allowed us to determine the effect of chemical stimulus on cell migration within the matrix, in the absence of other variables. FBS was employed as a chemoattractant.[59]

HT1080 cells—an invasive cancer cell model—were mixed with hydrogel precursor and injected into the main chamber of the microfluidic device

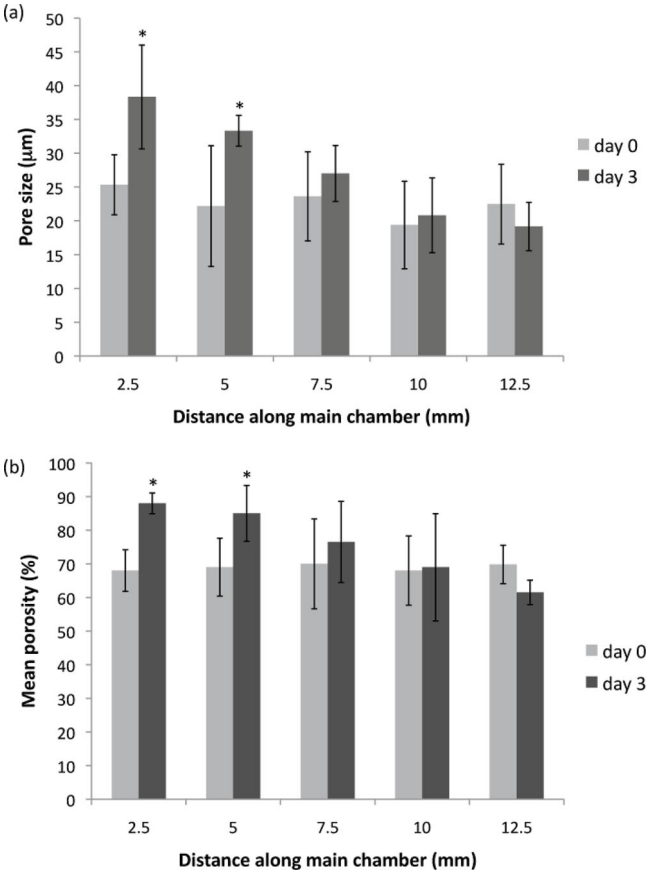

Figure 7. a) Pore size and b) porosity in five different regions from left to right of the porous hydrogel in the main chamber at day 0 and day 3 after addition of cellulase into the reservoir. At day 3, there is a decrease in the pore size and porosity from the left to the right of the hydrogel. Results are expressed as the mean value ± standard deviation (n = 6). P < 0.05 vs day 0 at the same region (*).

prior to gelation. A chemoattractant gradient was then generated over a 72-h period. The 3D-encapsulated HT1080 cells were then exposed to chemoattractant (FBS) provided in the right reservoir only, that is, the FBS concentration increased from the left to right regions of the main chamber. The cells were stained with LIVE/DEAD viability assay and imaged using LSCM to observe cell migration as well as cell viability. It can be seen from **Figure 8**a that many of the cells remained viable (thus appearing green) 12 h after hydrogel gelation. Between 12 and 72 h after chemoattractant was added, viable cells accumulated within the right hydrogel region of the main chamber so that relatively few or no cells remained in the center and left regions, respectively. This observation is consistent with the accumulation of cells toward the chemoattractant-rich regions on the right and is in agreement with numerous other studies, including those conducted in microfluidic devices, where cells preferentially migrated toward a chemoattractant.[60,61] Similar cell migration patterns were observed from optical microscopy images obtained after the hydrogel was lyophilized (Figure 8b). Most of the cells were stained by the LIVE viable stain in green indicating that these cells remained viable over the entire 72-h period of the experiment, and revealing that the in situ cell

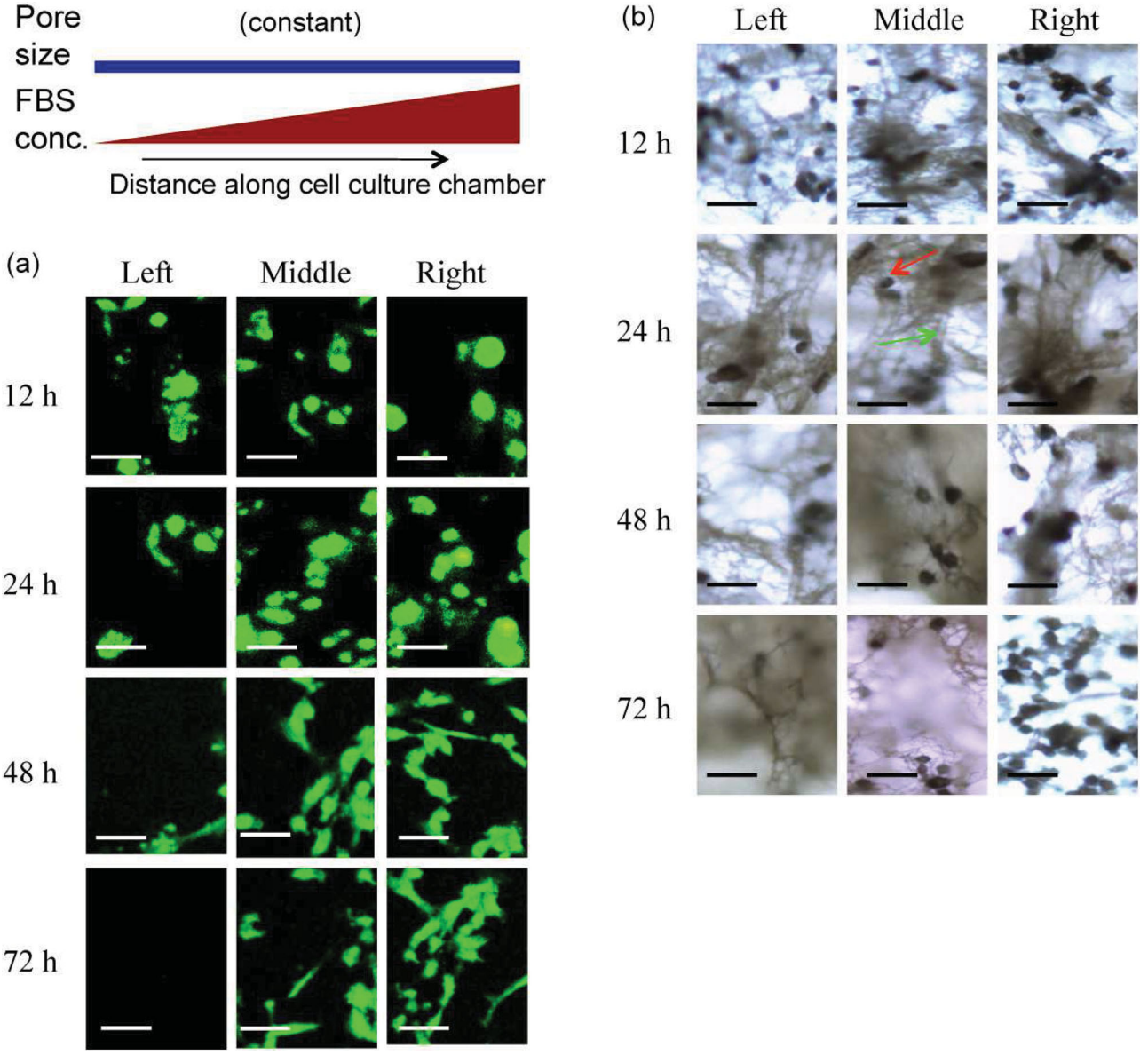

Figure 8. Case 1: Hydrogel containing a chemoattractant (FBS) gradient and homogeneous porosity and pore size as depicted by blue and red bars, respectively. a) Representative LSCM images showing the cell distribution in the left, middle, and right regions along the main chamber over a period of 72 h; the cells were stained using the LIVE/DEAD viability assay in a Calcein AM fluorescence channel. After 72 h, live cells (green) were observed to accumulate in the chemoattractant-rich, right side of the chamber. b) Representative optical microscopy images of the porous hydrogel in the main chamber after freeze-drying, showing the cell distribution within the hydrogel. The red arrow indicates the cells, whereas the green arrow indicates the freeze-dried hydrogel. The left, middle, and right regions were located 3, 9, and 12 mm, respectively, from the left side of the 15-mm long main chamber as depicted in Figure 2. Scale bars represent 50 μm.

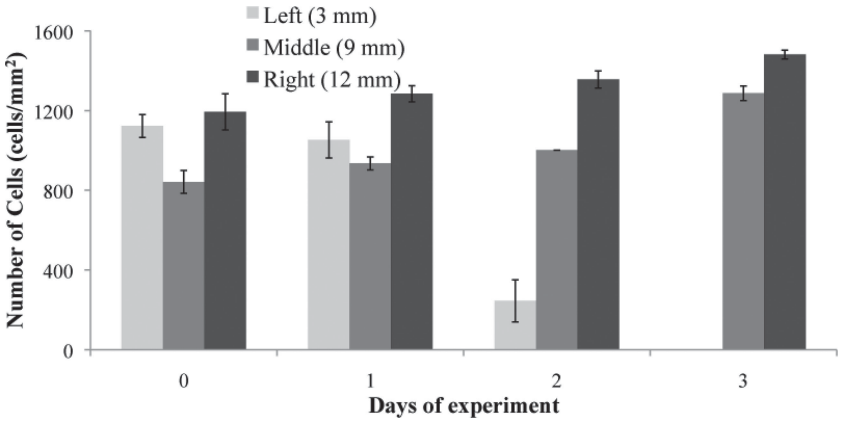

Figure 9. Quantification of the viable cell distribution within the main culture chamber containing the hydrogel after application of a chemoattractant (FBS) gradient with homogeneous porosity (Case 1). The left, middle, and right regions were located 3, 9, and 12 mm, respectively, from the left side of the 15-mm long main chamber as depicted in Figure 2. The error bars represent the standard deviation.

encapsulation process induces low cytotoxicity. Moreover, in our previous studies, the viability of COS-7 cells were found to be 93 ± 6.5% in the same GC hydrogel,[41] and neuroblasts were observed to migrated towards GC hydrogels injected into the subventricular zone of the brains of Wistar rats 7 d post-implantation.[62] These studies together with the present study thus confirmed the biocompatibility of the GC hydrogel.

Figure 9 shows results for the number of viable cells in each of the three regions (left, middle, and right) of the cell culture chamber, thus providing a quantitative histological view of the cell migration process over the 72-h period. The number of viable cells was slightly higher in the left and right regions compared to the middle region at day 0 (12 h after cell seeding), however, the differences are within typical experimental variation. As expected, the right region of the chamber contained the highest number of cells at day 3. At the same time, there was a significant decrease in the cell number relative to day 0 in the left region after 1, 2, and 3 d ($p < 0.0001$, $n = 4$). Despite the initial variability in cell density in the three regions, a trend of cell migration away from the left towards the right region can be seen in the figure if one compares the cell count for day 0 against day 3, thus demonstrating preferential cell migration toward the chemoattractant. Results obtained from counting the total number of cells in all three regions also showed similar migration patterns (Figure S1, Supporting Information).

3.3.2. Case 2: Cell Migration Along a Porosity Gradient with No Chemoattractant Gradient

Increasing evidence suggests that ECMs influence various cellular functions during cancer progression, morphogenesis, and normal development.[6] However, the underlying mechanisms involved are still not fully understood. There is thus a need for in vitro models that facilitate the study of how ECM regulates cell behavior. Although many mimetic culture systems have been developed for such studies, major challenges remain, particularly arising from the need to control the dynamics and spatial organization within these systems.[63]

Here, we demonstrate the potential of the GC hydrogel-based microfluidic device to provide dynamic and spatial control of the matrix structure. Specifically, we investigated using the microfluidic device the cellular response to a dynamic microenvironment in which the porosity varied with time. Over a 72-h period, a porous gradient was generated across the hydrogel by digesting the CMC component using cellulase enzyme. In this setup, cellulase was added to the left reservoir only so that a cellulase concentration gradient was generated within the hydrogel. As cellulase diffused across the main chamber, it generated and enlarged pores in the matrix by digesting CMC in a spatially controlled manner. As a result, the pore sizes and porosity decreased towards the middle and right regions of the hydrogel. Both left and right reservoirs were injected with the same amount of chemoattractant. In this case, a homogeneous chemoattractant concentration was maintained across the main chamber such that no specific cell migration under the influence of chemoattractant was induced. Again, most of the cells remained viable over the entire 72-h period, thus indicating that the process by which the porosity gradient was generated in situ-induced low cytotoxicity. This is consistent with observations from a previous study[41] where it was found that cellulase treatment did not induce any toxicity effects on cells.

It can be seen from **Figure 10**a that at day 0, cells were uniformly distributed within the main chamber given that both left and right reservoirs were supplied with the same amount of medium, demonstrating that application of the in situ synthesized GC hydrogel overcomes the difficulties in achieving homogeneous cell distributions that often occur when preformed hydrogel structures are used in microfluidic devices. As seen in the images obtained using LSCM in Figures 6 and 10a, the pore size appears to have a significant effect on cell migration within the scaffold. Over a 72-h period, the cells were observed to accumulate in the region with the largest pore size (left region in the main chamber). Such preferential migration in spatially complex matrices from more tightly confined porous regions to larger open porous regions may also occur in ECM microenvironments in real living tissue, although this is not consistent with the suggestion of Tripathi et al.,[34] that smaller pores provide larger surface area, which allows for more cell growth; nevertheless, we note that the present pore size range is different from that of Tripathi et al. (45–180 μm). A study of the mechanical properties in our previous work showed that the storage modulus (an indicator of stiffness)[39] of the same GC hydrogel decreased from 3741 to 2788 Pa after cellulase digestion due to loss of cellulose mass, which is associated with larger pore sizes.[41] The decrease in the storage modulus with increasing pore size and porosity in the GC hydrogel after cellulase digestion[41] thus means that our observation here that cells migrate to

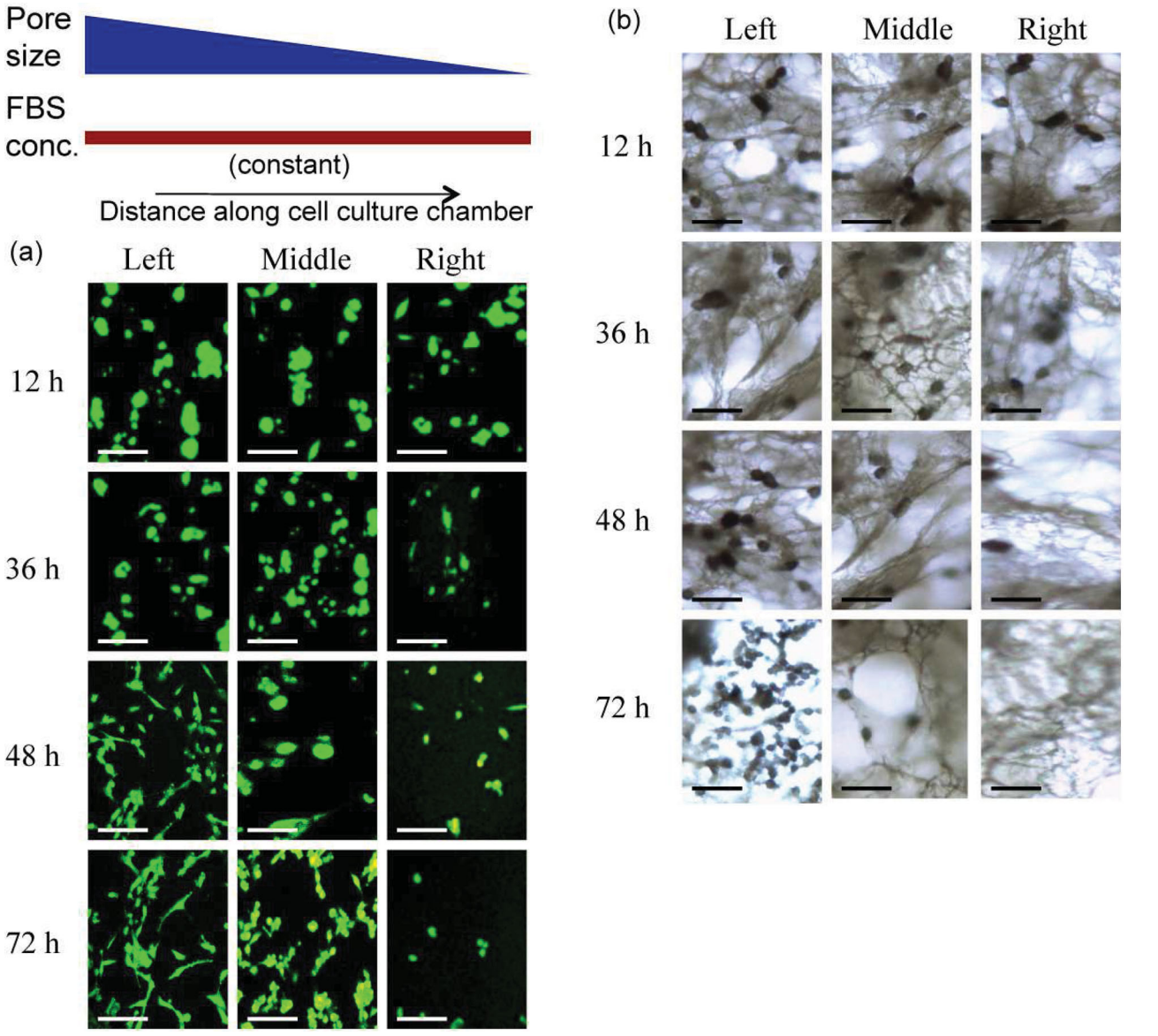

Figure 10. Case 2: Hydrogel containing a porosity/pore size gradient and no chemoattractant gradient as depicted by blue and red bars, respectively. a) Representative LSCM images showing the cell distribution in the left, middle, and right regions along the main chamber over a period of 72 h; the cells were stained using the LIVE/DEAD viability assay in a Calcein AM fluorescence channel. After 72 h, live cells (green) were observed to accumulate in the left region of the chamber where the pores were largest. b) Representative optical microscopy images of the porous hydrogel in the main chamber after freeze-drying, showing the cell distribution within the hydrogel. The left, middle, and right regions were located 3, 9, and 12 mm, respectively, from the left side of the 15-mm long main chamber as depicted in Figure 2. Scale bars represent 50 µm.

regions of lower stiffness is in contrast to their behavior during durotaxis or mechanotaxis[1] when cells are known to migrate toward stiffer regions on 2D hydrogels.[64] Our results therefore suggest that the influence of 3D porosity on cell migration could override that due to matrix stiffness. After 72 h, the shape of the cells in the left region appeared to be elongated compared to that of the cells in the middle and right regions of the chamber, suggesting that the cells settled and spread in the presence of larger pores. This observation is similar to that of Lin et al.,[15] where cells appeared more well-spread in larger pores compared to those in smaller pores.

Figure 10b shows the porous gradient hydrogel containing cells after lyophilization. These images of the lyophilized scaffold provided further confirmation that the cells accumulated in the left region of the culture chamber, again indicating that the larger pores allowed for improved cellular infiltration. The quantitative data in **Figure 11** show that, after 3 d, the left region of the main chamber contained the highest average number of viable cells compared to the middle ($p < 0.0001$, $n = 4$) and right region ($p < 0.0001$, $n = 4$), and that there was a significant reduction in the cell numbers in the right regions ($p < 0.0001$, $n = 4$) of the main chamber over the duration of the experiment. Results obtained from counting the total number

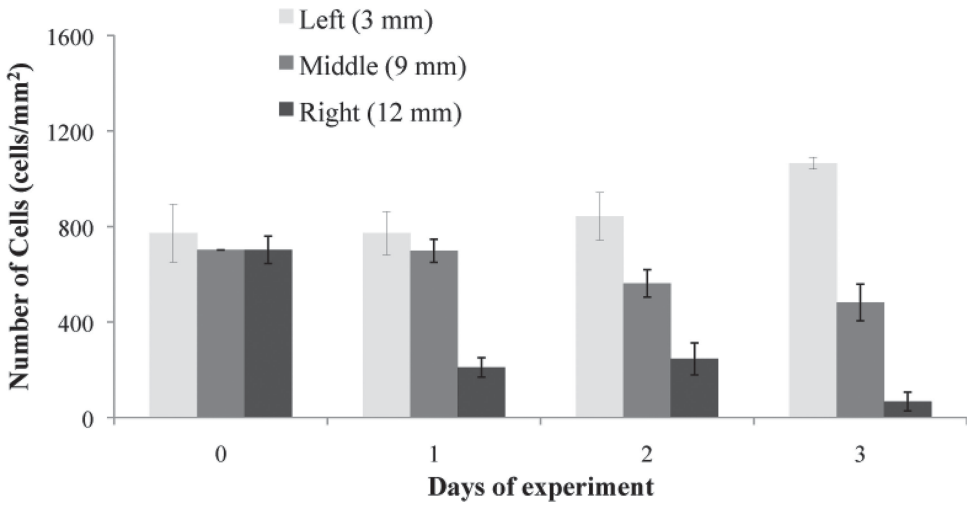

Figure 11. Quantification of the cell distribution within the main culture chamber containing the hydrogel after application of a porosity gradient but in the absence of a chemoattractant (FBS) gradient (Case 2). The left, middle, and right regions were located 3, 9, and 12 mm, respectively, from the left side of the 15-mm long main chamber as depicted in Figure 2. Each error bar represents the standard deviation of the mean.

of cells in all three regions also showed similar migration patterns (Figure S2, Supporting Information). Altogether, these results demonstrate that the mean pore size had a significant effect on cell migration and that regions of the scaffold with the largest pores accumulated the highest cell density.

3.3.3. Case 3: Cell Migration Along a Porosity Gradient in the Presence of a Chemoattractant Gradient

Morphogenesis is a complex process in which both ECM remodeling and chemotaxis can occur simultaneously.[6] An in vitro model that permits in situ tuning of both porosity and chemical gradients is therefore valuable for studying morphogenesis. In Case 3, cell behavior was investigated under the influence of two different gradients, that is, a porosity gradient and a chemoattract gradient were generated in situ after cell immobilization in the microfluidic device. The gradients were generated in such a way that the porosity increased towards the left side of the main chamber while the chemoattractant concentration increased towards the right side as depicted in **Figure 12**.

It can be observed in Figure 12a that cells were distributed quite uniformly within the main chamber 12 h after hydrogel gelation. As the gradients were being generated, the cells appeared to be drawn toward the middle region from both the left and right regions at 48 h, given that the pores were larger in the middle region compared to those in the right region, and since the concentration of chemoattractant in the middle region was higher compared to that in the left region. Most of the cells eventually settled in the middle region after 72 h, suggesting that both pore size and chemoattractant played a crucial role in migration of the cells. Figure 12b shows the hydrogel containing cells after freeze-drying and confirms the development with time of a relatively high density of cells in the middle region. The quantitative data in **Figure 13** show that at day 0 (12 h after cell seeding), the number of viable cells in the left and middle regions was slightly lower compared to that in the right region, however, the differences are within typical experimental variation. Despite the initial variability in cell density in the three regions, a trend of cell migration toward the middle region can be seen in the figure if one compares the cell count for day 0 against subsequent days. The middle region contained the highest average number of cells compared to the left ($p < 0.0001$, $n = 4$) and middle ($p < 0.0001$, $n = 4$) regions after 72 h, and that there was a significant reduction in cell numbers in the left ($p < 0.0001$, $n = 4$) and right regions ($p < 0.0001$, $n = 4$) of the main chamber over the duration of the experiment. Similar migration patterns can be observed in Figure S3 (Supporting Information) showing the total number of cells in all three regions.

This study thus demonstrates the feasibility of the GC hydrogel-based microfluidic device for the generation of both porosity and concentration gradients in situ after cell immobilization. More importantly, the study shows that cellular responses to a dynamically and spatially changing matrix can be monitored in real time using this system. In future studies, instead of continuously applying cellulase digestion, multiple applications of cellulase may be used to increase the porosity at selected time points to mimic different phases of ECM remodeling during cell differentiation and tissue development. The concentration of cellulase could also be varied to modulate the rate of pore digestion to mimic different ECM remodeling rates. Additionally, a more complex gradient generation network[65] could be incorporated into this GC hydrogel-based microfluidic system to generate other complex porosity and biochemical gradient environments to elicit different in vivo tissue behavior.

4. Conclusions

A significant limitation of chemotaxis studies to date lies in their inability to accurately mimic the physiologically and chemically

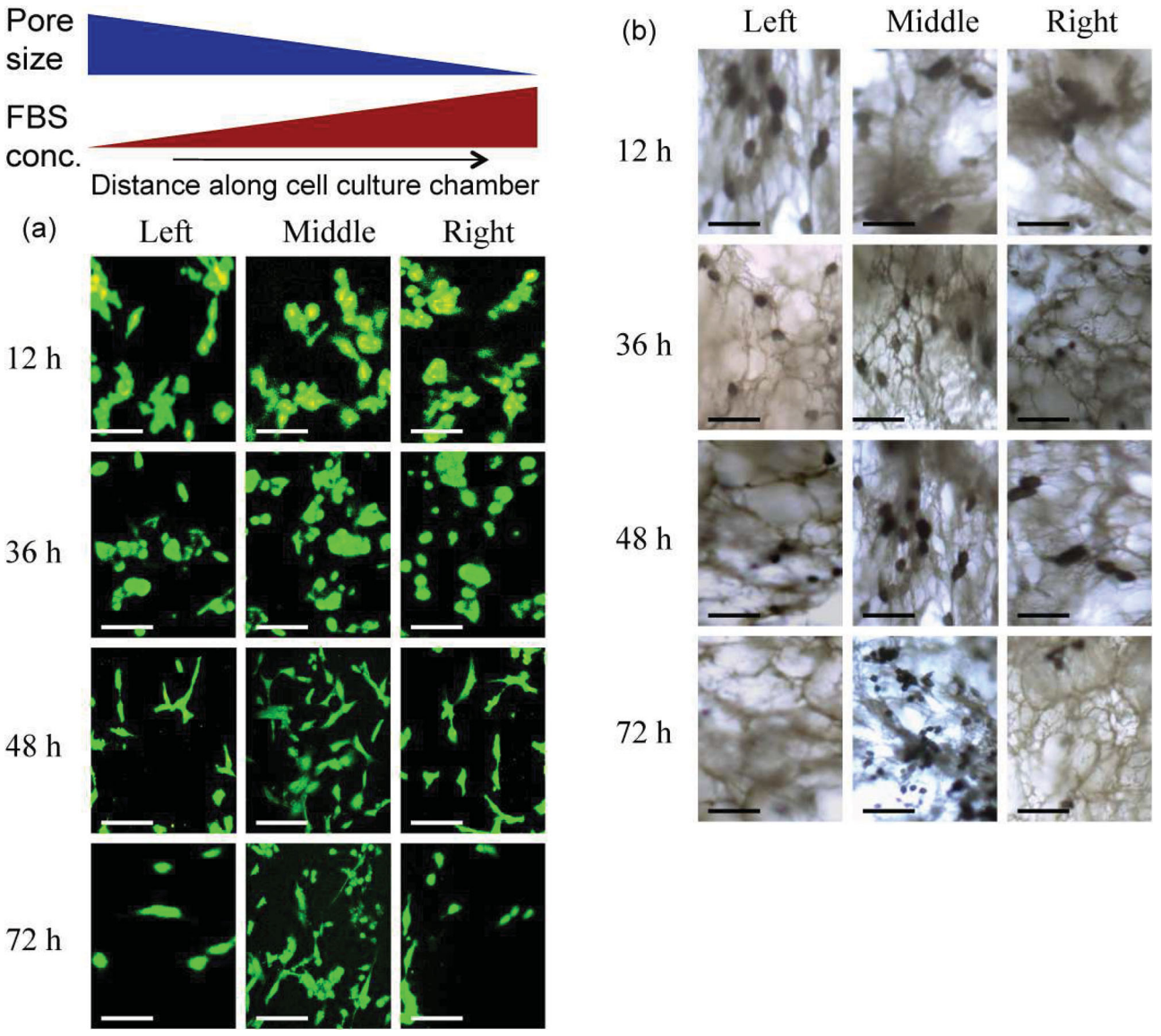

Figure 12. Case 3: Hydrogel containing overlapping chemoattractant (FBS) and porosity gradients as depicted by blue and red bars, respectively. a) Representative LSCM images showing the cell distribution in the left, middle, and right regions along the main chamber over a period of 72 h; the cells were stained using the LIVE/DEAD viability assay in a Calcein AM fluorescence channel. After 72 h, live cells (green) were observed to accumulate in the middle region. b) Representative optical microscopy images of the porous hydrogel in the main chamber after freeze-drying, showing the cell distribution within the hydrogel. The left, middle, and right regions were located 3, 9, and 12 mm, respectively, from the left side of the 15-mm long main chamber as depicted in Figure 2. Scale bars represent 50 µm.

relevant features of in vivo microarchitecture, in particular, the dynamic microenvironment as it undergoes structural change. We have addressed this limitation by developing a hydrogel-based microfluidic platform that allows cells to be embedded with uniform cell density in a porous 3D GC hydrogel scaffold, and subsequently using this platform to monitor the chemotactic response of HT1080 cancer cells under the influence of a matrix with varying pore size. The dynamic pore structure was achieved after formation of the scaffold and immobilization of cells by tuning the hydrogel porosity in situ using cellulase enzyme. This feature is not available using current methods for generating porous gradients in biomaterials comprising preformed structures.

A continuous porosity gradient was generated in situ within hydrogel containing cells in a microfluidic culture chamber. The results showed that cellular migration is sensitive to the hydrogel pore size, with cells migrating along the scaffold toward the largest pores in the absence of chemoattractant. However, when chemoattractant is present in addition to the gradient in porosity, the cells were attracted both to the chemoattractant in one direction and towards the region of larger pores in the opposite direction, resulting in a region of high cell density in the middle of the cell culture chamber. The microfluidic platform presented here, which incorporates the use of perfusable hydrogels with complementary

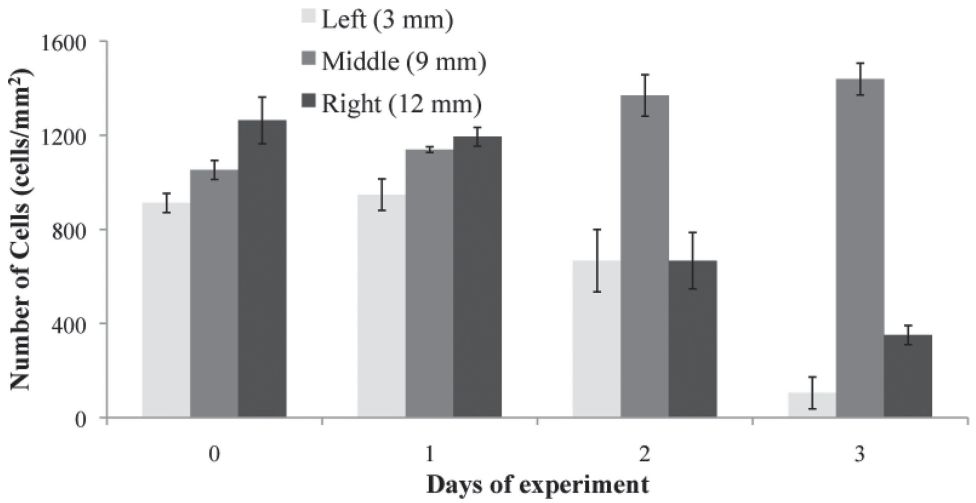

Figure 13. Quantification of the cell distribution within the main culture chamber containing the hydrogel with overlapping porosity and chemoattractant (FBS) gradients (Case 3). The left, middle, and right regions were located 3, 9, and 12 mm, respectively, from the left side of the 15-mm long main chamber as depicted in Figure 2. Each error bar represents the standard deviation of the mean.

photolithographic fabrication methodologies, demonstrates the potential for the development of robust culture systems for the construction of complex, microscale, biomimetic, and in vitro tissue analogues.

Supporting Information

Supporting Information is available from the Wiley Online Library or from the author.

Acknowledgements

Funding for this work was partly provided through Australian Research Council Discovery Grants DP 120102570 and DP 120100013. This work was performed in part at the Melbourne Centre for Nanofabrication (MCN) which comprises the Victorian Node of the Australian National Fabrication Facility (ANFF). L.Y.Y. gratefully acknowledges funding support through the Australian Research Fellowship from the Australian Research Council as part of Discovery Project grant DP098525. J.R.F. is grateful for an MCN Senior Technology Fellowship and an RMIT Vice-Chancellor's Senior Research Fellowship. P.P.Y.C. is grateful for an MCN Technology Fellowship and an RMIT Senior Research Fellowship.

Received: February 2, 2014
Revised: March 9, 2014
Published online: April 7, 2014

[1] S. Sant, M. J. Hancock, J. P. Donnelly, D. Iyer, A. Khademhosseini, *Can. J. Chem. Eng.* **2010**, *88*, 899.
[2] S. P. Ho, B. Yu, W. Yun, G. W. Marshall, M. I. Ryder, S. J. Marshall, *Acta Biomater.* **2009**, *5*, 707.
[3] S. P. Ho, M. P. Kurylo, T. K. Fong, S. S. J. Lee, H. D. Wagner, M. I. Ryder, G. W. Marshall, *Biomaterials* **2010**, *31*, 6635.
[4] S. P. Ho, P. Senkyrikova, G. W. Marshall, W. Yun, Y. Wang, K. Karan, C. Li, S. J. Marshall, *Dental Mater.* **2009**, *25*, 1195.
[5] L. M. Reid, A. S. Fiorino, S. H. Sigal, S. Brill, P. A. Holst, *Hepatology* **1992**, *15*, 1198.
[6] T. Rozario, D. W. DeSimone, *Dev. Biol.* **2010**, *341*, 126.
[7] S. Q. Liu, Q. Tian, J. L. Hedrick, J. H. Po Hui, P. L. Rachel Ee, Y. Y. Yang, *Biomaterials* **2010**, *31*, 7298.
[8] U. Haessler, J. C. M. Teo, D. Foretay, P. Renaud, M. A. Swartz, *Integrative Biol.* **2012**, *4*, 401.
[9] K. S. Midwood, L. V. Williams, J. E. Schwarzbauer, *Int. J. Biochem. Cell Biol.* **2004**, *36*, 1031.
[10] F. Z. Volpato, T. Führmann, C. Migliaresi, D. W. Hutmacher, P. D. Dalton, *Biomaterials* **2013**, *34*, 4945.
[11] P. Brun, G. Abatangelo, M. Radice, V. Zacchi, D. Guidolin, D. D. Gordini, R. Cortivo, *J. Biomed. Mater. Res.* **1999**, *46*, 337.
[12] S. E. McGowan, *FASEB J.* **1992**, *6*, 2895.
[13] B.-S. Kim, I.-K. Park, T. Hoshiba, H.-L. Jiang, Y.-J. Choi, T. Akaike, C.-S. Cho, *Prog. Polym. Sci.* **2011**, *36*, 238.
[14] B. A. Harley, A. Z. Hastings, I. V. Yannas, A. Sannino, *Biomaterials* **2006**, *27*, 866.
[15] J.-y. Lin, W.-j. Lin, W.-h. Hong, W.-c. Hung, S. H. Nowotarski, S. M. Gouveia, I. Cristo, K.-h. Lin, *Soft Matter* **2011**, *7*, 10010.
[16] X. Miao, D. Sun, *Materials* **2009**, *3*, 26.
[17] J. Werner, B. Linner-Kr mar, W. Friess, P. Greil, *Biomaterials* **2002**, *23*, 4285.
[18] A. Muthutantri, J. Huang, M. Edirisinghe, *J. R. Soc. Interface* **2008**, *5*, 1459.
[19] A. Macchetta, I. G. Turner, C. R. Bowen, *Acta Biomater.* **2009**, *5*, 1319.
[20] L. Y. Yeo, H.-C. Chang, P. P. Y. Chan, J. R. Friend, *Small* **2011**, *7*, 12.
[21] J. C. McDonald, D. C. Duffy, J. R. Anderson, D. T. Chiu, H. Wu, O. J. A. Schueller, G. M. Whitesides, *Electrophoresis* **2000**, *21*, 27.
[22] O. E. Shklyaev, A. Q. Shen, *Mech. Res. Commun.* **2009**, *36*, 121.
[23] S. Kim, H. J. Kim, N. L. Jeon, *Integrative Biol.* **2010**, *2*, 584.
[24] F. Lin, in Methods in Enzymology, Vol. *461* (Eds: M. H. Tracy, J. H. Damon), Academic Press, San Diego, USA **2009**, 333.
[25] K. Kreppenhofer, J. Li, R. Segura, L. Popp, M. Rossi, P. Tzvetkova, B. Luy, C. J. Kähler, A. E. Guber, P. A. Levkin, *Langmuir* **2013**, *29*, 3797.
[26] N. L. W. Franssen-van Hal, J. E. Bunschoten, D. P. Venema, P. C. H. Hollman, G. Riss, J. Keijer, *Arch. Biochem. Biophys.* **2005**, *439*, 32.
[27] J. He, Y. Du, J. L. Villa-Uribe, C. Hwang, D. Li, A. Khademhosseini, *Adv. Funct. Mater.* **2010**, *20*, 131.

[28] M. Bok, H. Li, L. Y. Yeo, J. R. Friend, *Biotechnol. Bioeng.* **2009**, *103*, 387.
[29] H. Li, J. R. Friend, L. Y. Yeo, *Biomaterials* **2007**, *28*, 4098.
[30] J. J. A. Barry, D. Howard, K. M. Shakesheff, S. M. Howdle, M. R. Alexander, *Adv. Mater.* **2006**, *18*, 1406.
[31] J. J. A. Barry, M. M. C. G. Silva, K. M. Shakesheff, S. M. Howdle, M. R. Alexander, *Adv. Funct. Mater.* **2005**, *15*, 1134.
[32] L. Kim, Y.-C. Toh, J. Voldman, H. Yu, *Lab Chip* **2007**, *7*, 681.
[33] S. H. Oh, I. K. Park, J. M. Kim, J. H. Lee, *Biomaterials* **2007**, *28*, 1664.
[34] A. Tripathi, N. Kathuria, A. Kumar, *J. Biomed. Mater. Res. Part A* **2009**, *90A*, 680.
[35] P. Dubruel, R. Unger, S. Van Vlierberghe, V. Cnudde, P. J. S. Jacobs, E. Schacht, C. J. Kirkpatrick, *Biomacromolecules* **2007**, *8*, 338.
[36] Q. Zhang, H. Lu, N. Kawazoe, G. Chen, *Mater. Lett.* **2013**, *107*, 280.
[37] C. M. Murphy, M. G. Haugh, F. J. O'Brien, *Biomaterials* **2010**, *31*, 461.
[38] F. J. O'Brien, B. A. Harley, I. V. Yannas, L. J. Gibson, *Biomaterials* **2005**, *26*, 433.
[39] L.-S. Wang, J. E. Chung, P. P.Y. Chan, M. Kurisawa, *Biomaterials* **2010**, *31*, 1148.
[40] F. Sarvi, Z. Yue, K. Hourigan, M. C. Thompson, P. P. Y. Chan, *J. Mater. Chem. B* **2013**, *1*, 987.
[41] A. Al-Abboodi, J. Fu, P. M. Doran, T. T. Y. Tan, P. P. Y. Chan, *Adv. Healthcare Mater.* **2013**, DOI:10.1002/adhm.201300303.
[42] A. Al-Abboodi, J. Fu, P. M. Doran, P. P. Y. Chan, *Biotechnol. Bioeng.* **2013**, *110*, 318.
[43] E. Maquoi, A. Noël, F. Frankenne, H. Angliker, G. Murphy, J.-M. Foidart, *FEBS Lett.* **1998**, *424*, 262.
[44] J. Friend, L. Yeo, *Biomicrofluidics* **2010**, *4*, 026502.
[45] L.-S. Wang, J. Boulaire, P. P. Y. Chan, J. E. Chung, M. Kurisawa, *Biomaterials* **2010**, *31*, 8608.
[46] M. Hu, M. Kurisawa, R. Deng, C. M. Teo, A. Schumacher, Y. X. Thong, L. Wang, K. M. Schumacher, J. Y. Ying, *Biomaterials* **2009**, *30*, 3523.
[47] D. E. Garfin, *TrAC Trends Anal. Chem.* **2003**, *22*, 263.
[48] J. Wu, Q. Chen, W. Liu, Y. Zhang, J.-M. Lin, *Lab Chip* **2012**, *12*, 3474.
[49] L. J. Millet, M. E. Stewart, R. G. Nuzzo, M. U. Gillette, *Lab Chip* **2010**, *10*, 1525.
[50] T. M. Keenan, A. Folch, *Lab Chip* **2008**, *8*, 34.
[51] M. K. Kalra, M. S. Sidhu, D. K. Sandhu, *J. Appl. Bacteriol.* **1986**, *61*, 73.
[52] G. Shouren, K. Kojio, A. Takahara, T. Kajiyama, *J. Biomat. Sci.-Polym. E.* **1998**, *9*, 131.
[53] E. Ahlgren, K.-E. Eriksson, O. Vesterberg, *Acta Chem. Scand.* **1967**, *21*, 937.
[54] S. P. Hoo, Q. L. Loh, Z. Yue, J. Fu, T. T. Y. Tan, C. Choong, P. P. Y. Chan, *J. Mater. Chem. B* **2013**, *1*, 3107.
[55] J. Klominek, K.-H. Robert, K.-G. Sundqvist, *Cancer Res.* **1993**, *53*, 4376.
[56] C. Janetopoulos, R. A. Firtel, *FEBS Lett.* **2008**, *582*, 2075.
[57] E. K. Frow, J. Reckless, D. J. Grainger, *Med. Res. Rev.* **2004**, *24*, 276.
[58] A. Qi, S. P. Hoo, J. Friend, L. Yeo, Z. Yue, P. P. Y. Chan, *Adv. Healthc. Mater.* **2013**, n/a.
[59] C. Barthomeuf, S. Lamy, M. Blanchette, D. Boivin, D. Gingras, R. Béliveau, *Free Radical Biol. Med.* **2006**, *40*, 581.
[60] S.-J. Wang, W. Saadi, F. Lin, C. Minh-Canh Nguyen, N. Li Jeon, *Exp. Cell Res.* **2004**, *300*, 180.
[61] U. Haessler, Y. Kalinin, M. Swartz, M. Wu, *Biomed. Microdevices* **2009**, *11*, 827.
[62] D. Fon, A. Al-Abboodi, P. P. Y. Chan, K. Zhou, P. Crack, D. I. Finkelstein, J. S. Forsythe, *Adv. Healthcare Mater.* **2014**.
[63] M. P. Lutolf, J. A. Hubbell, *Nat. Biotechnol.* **2005**, *23*, 47.
[64] M. Ehrbar, A. Sala, P. Lienemann, A. Ranga, K. Mosiewicz, A. Bittermann, S. C. Rizzi, F. E. Weber, M. P. Lutolf, *Biophys. J.* **2011**, *100*, 284.
[65] D. Irimia, S.-Y. Liu, W. G. Tharp, A. Samadani, M. Toner, M. C. Poznansky, *Lab Chip* **2006**, *6*, 191.